Is the curvature of the flagellum involved in the apparent cooperativity of the dynein arms along the "9+2" axoneme?

Christian Cibert, Andrei Ludu

Is the curvature of the flagellum involved in the apparent cooperativity of the dynein arms along the "9+2" axoneme?

Christian Cibert, Andrei Ludu

PII: S0022-5193(10)00187-6
DOI: doi:10.1016/j.jtbi.2010.04.004
Reference: YJTBI5953

To appear in: *Journal of Theoretical Biology*

Received date: 31 May 2009
Revised date: 25 March 2010
Accepted date: 6 April 2010

Cite this article as: Christian Cibert and Andrei Ludu, Is the curvature of the flagellum involved in the apparent cooperativity of the dynein arms along the "9+2" axoneme?, *Journal of Theoretical Biology*, doi:10.1016/j.jtbi.2010.04.004

IS THE CURVATURE OF THE FLAGELLUM INVOLVED IN THE APPARENT COOPERATIVITY OF THE DYNEIN ARMS ALONG THE "9+2" AXONEME?

Christian Cibert[1] and **Andrei Ludu**[2]

[1] Author for correspondence, Er 3 "Biogenèse Des Signaux Peptidiques", University Paris 6, 2, place Jussieu, F-75252 Paris, France. Present address: UVSQ, LISV, Centre Universitaire de Technologie, laboratoire de robotique des explorations, 10/12 Avenue de l'Europe, F-78140 Velizy, France. Phone: 33 (0)6 77 13 46 71, e-mail: cibert@lisv.uvsq.fr or cibert.christian@wanadoo.fr.

[2] Dept. Chemistry and Physics, Northwestern State University, Natchitoches, LA 71497, USA.

Running title: cooperativity of the dynein arms within the axoneme

Key words : axoneme, cooperativity, dynein arms, flagellum, topology

SUMMARY

In a recent study (Cibert, C. (2008), Journal of Theoretical Biology, 253: 74-89), by assuming that the walls of the microtubules are involved in cyclic compression/dilation equilibriums as a consequence of the cyclic curvature of the axoneme, it was proposed that the local adjustments of the spatial frequencies of both the dynein arms, and the β-tubulin monomers facing series, create the propagation of joint probability waves of interaction (JPI) between these two necessary partners. Modeling the occurrence of these probable interactions along the entire length of an axoneme between each outer doublet pairs (without programming any cooperative dialog between the molecular complexes) and the cyclic attachment of two facing partners, we show that the active couples such constituted are clustered. Along a cluster the dynein arms exhibit a small phase shift with respect to the order according to which they began each their cycle after being linked to a β-tubulin monomer. The numbers of couples included in these clusters depend on the probability of interaction between the dynein arms and the β-tubulin, on the location of the outer doublet pairs around the axonemal cylinder, and on the local bending of the axoneme; around the axonemal cylinder, the faster and larger the sliding, the shorter the clusters. This mechanism could be involved in the apparent cooperativity of the molecular motors and the β-tubulin monomers, since it is partially controlled by the local curvature, and the cluster length is inversely proportional to the sliding activity of the outer doublet pairs they link.

INTRODUCTION

The motile axis of the flagella and cilia of the eukaryotic cells — the axoneme — is formed by nine outer doublets of microtubules constituting 9 Outer Doublet Pairs (ODPs), which surround a central apparatus organized around two central microtubules. Because of the

activity the dynein arms (DAs), and the existence of elastic links interconnecting the ODPs, the relative shear of the ODPs is converted into bends (Gibbons, 1981; Lindemann, 1994a). The local curvature of such bends may be associated with the twist of the axonemal cylinder around its central axis (Cibert, 2001; Gibbons, 1975).

The nature of the instantaneous regulation of this mechanism, which allows the propagation of a coherent wave train along these organelles, is basically unknown in spite of the existence of clever biochemical and topologic models. Such models consider the curvature and the geometrical adjustments of the axonemal machinery to be essential for the functioning of the ensemble of diverse mechanisms (Brokaw, 1975; Dymek and Smith, 2007; Gertsberg et al., 2004; Huang et al., 1982; Inaba, 2003; Li et al., 2006; Lindemann, 1994a; Lindemann, 2007; Lindemann and Mitchell, 2007; Mitchell, 2003a; Mitchell, 2003b; Morita et al., 2006; Morita and Shingyoji, 2004; Noguchi et al., 2000; Noguchi et al., 2005; Piperno et al., 1992; Rupp and Porter, 2003; Smith and Yang, 2004; Wilson and Lefebvre, 2004; Woolley, 2007; Woolley, 1997).

In parallel to these biological models, physical ones assume that the couples "ODPs – molecular motors" produce alternative fields of internal constraints during the beating movements. One of the most interesting hypothesis is the pioneering description of these active entities as "auto-driven filaments" (Camalet et al., 1999). These models postulate that the efficient DAs are uniformly distributed along each ODP, and they produce forces along the entire length of the ODPs. However, experimental observations suggest that the DAs are active when they are associated in clusters of 4 elements (Spungin et al., 1987) making the DAs and their partners to become cooperative systems in essence. Here, cooperativity is defined as the necessary inter-molecular dialog occurring either inside a given molecular complex, or between different molecular complexes, as in the case of allosteric enzymes.

From the known range of the physical characteristics (elastic constants) of the microtubules and of the ODPs (Fujime et al., 1972; Schoutens, 1994; Takano et al., 2003) one can assume that microtubules are inextensible and incompressible in the limits of normal beating cycles. However, different arguments plead in favor of their deformations during the beating cycles. This allows us to bring the hypothesis that two opposite sides of the outer doublets included in the bending plane are subjected to dilation/compression equilibrium controlled by the local balance of forces and torques (Cibert, 2008). From the above discussion and the assumption that dilation/compression sequences modulate the periodic distributions of the DAs and the β-TM along the two facing verniers during a beating cycle, the joint probability of interaction (JPI) of the facing DAs and β-TM depends on: (i) the local curvature, (ii) the local rate of sliding, and (iii) the location of the ODPs within the axoneme, all these three factors being taken into account relative to the orientation of the bending plane (Cibert, 2008).

The JPI wave trains are created by the relative displacements of the two molecular verniers, whose shearing could be positive, negative or nil, and whose special frequencies vary with respect to the local curvature of the model. Thus, the "sampling" of one vernier by the other (and conversely), *i.e.* the coincidence between their facing elements, is stroboscopic in essence, and the apparent displacement of the JPI wave train could be tipward, baseward or nil, as a function of the values of the physical parameters that generate them, and not as a function of the polarity of the shear only (Cibert, 2008).

In the present paper, assuming that orientation of the bending plane is constant along the entire length of the model, the distribution of the couples DAs – β-TMs along the nine ODPs during a beating cycle was modeled. These distributions are highly heterogeneous

around, and along the axonemal cylinder. The active couples tend to form cluster series along the 9 ODPs in relation to the sliding speed, the local bending and the cylindrical location of the ODPs.

These results confirm two things: first, that the geometry could be one of the major elements involved in the definition of the apparent cooperativity existing between DAs and β-TMs during the axonemal beating, and second, that this cooperativity must be considered as adaptative because it depends on the local curvature and on the location of the outer doublet pairs around the axonemal cylinder.

MATERIAL, CALCULATIONS AND ASSUMPTIONS

The program was written under ImageJ (1.37v) running on a MacBook Pro (Intel) OS-X platform (rsbweb.nih.gov/ij/download.html).

According to Gray (Gray, 1955; Gray, 1958; Gray and Hancock, 1955), traces of the flagellum of a sea urchin spermatozoon (chosen as model) were calculated as the products of an exponential envelope and a periodic function (Cibert, 2008), whose equations are $y_1=a_0*(1-\exp(-a_1x))$ and $y_2=\sin(w(kt-x/v)+\varphi)$, respectively, where: $a_0=100$, $a_1=2$, $w=0.8$, $v=0.31$, $k=r*8/160$, $\varphi=-23\pi/80+\varphi_0$, x is the abscissa containing the 200 points of sampling of the traces that ranges on the interval [0, 3], r is the rank of the trace in the beating cycle (Figure 1), and 160 is the number of traces that constitute the complete beating cycle. The abscissa x is calculated as $x=i*3/200$, where i is the rank of the sampling point ranging in the interval [0, 200]. In the periodic function the quantities k and x/v are related to the displacement of the wave train along the longitudinal direction, as a function of time, and describe the shape of the wave train for a given moment of time, respectively. Values of the other parameters are chosen to mimic the beating of sea urchin spermatozoon. The length of each trace equals 40 μm. If the beating frequency of the model is 50 Hz the interval between two images of the bending series becomes 1/8,000 s. One image out of ten is displayed along the series in Figure 1 A-B where φ_0 equals 0 and $\pi/2$, respectively (higher ranks are identified by darker traces).

The range of the local shear calculated along each of the 160 traces is characterized by a fish-shaped envelope, in agreement with earlier descriptions (Figure 1 C) (Cibert, 2002). This plot characterizes the P0 points as the curvilinear abscissas, where the relative shear of the ODPs tends to a minimum, because of the synchronous (Brokaw, 1996; Brokaw, 1993; Goldstein, 1976) and cumulative (Cibert, 2001; Cibert, 2002; Cibert, 2003) sliding of the ODPs. Consequently, the wave train moving along the axoneme delineates a series of P0-P0 modules along the model (Cibert, 2002), and the shear of the ODPs along the entire length of the axoneme occurs irrespectively of the local curvature (Cibert, 2002; Cibert, 2008).

Figure 2 shows the cross section of the axoneme that we have used in this study, and the magnitude of compression and the dilation of the intervals that separate two successive tubulin monomers and dynein arms when a 10 μm long segment of the axoneme bends and the angle equals π (Cibert, 2008).

The incidence of the JPI wave trains on the distribution of the active DA along, and around the axoneme, was calculated assuming that dynein arms could tilt baseward or tipward (Figure 3). In this scheme, the arbitrary correspondence between the tilt of the dynein arms and their colors was used. Namely, the dynein arms is represented white when it is

perpendicular to the wall of the doublet on which it is constitutively fixed (stand-by position, or the beginning of the walking cycle of the arm); it becomes darker through a range of red colors when its tilt increases on the two sides of the stand-by conformation. The couples DA – β-TM are preserved during the shear reversion. Figure 3 shows that the DAs whose tilt angles are comparable form clusters of different sizes along the ODPs. Five abscissas of interest taken along the modeled axoneme were considered (Figure 1 C).

RESULTS AND DISCUSSION

From the knowledge of a flagellar wave train and the corresponding sliding of the axonemal cylinder based on the model already described in Cibert (2008), the formation of the couples DA – β-TM was calculated according to six principles. (i) The ODP shear is zero at the basal anchor of the axoneme. (ii) The beating plane is constant and stable, and it contains the doublet #1 and the axis of the model. (iii) Maximum length of a step taken by the DAs is assumed to be 160 Å. (iv) The link between a given DA and a facing β-TM is triggered by the local occurrence of the JPI wave train, through its propagation along each ODP (Cibert, 2008) — the tables describing the propagation of the JPI wave train are the ones shown in that paper. (v) The four mechano-chemical steps of the DAs (Omoto et al., 1991) are converted into a turn-off (stand-by activated position), a turn-on (linked to a β-TM) conformation, and a continuous series of tilted conformations between these two extrema. (vi) One DA turns-off and detaches from its partner when it reaches its maximum walking capabilities, assuming that the maximum tilt angle of a DA has the same amplitude in both directions (Gennerich et al., 2007; Lindemann and Hunt, 2003; Lorch et al., 2008).

The polarity of the propagation of the JPI wave trains along the axoneme describes solely the spatial coincidence of each of the elements of the two facing verniers, without any condition associated to their effective binding. As a function of the ratio between the rate of displacement of the JPI wave train and the lifetime of each active couple DA – β-TM, the spatial coincidences between the two partners may or may not induce linking between them; a link is created only when the facing molecules are free. This means that if either a DA or a β-TM involved in an active couple faces exactly a free partner, grasping does not occurs because it is still working.

For simplicity, only the behavior of the couples DA – β-TM along one segment of interest is presented (#2 in Figure 1 C); this curvilinear abscissa is the geometrical locus where the shear amplitude is the highest along the model. The other time series (Figure 1 C) are presented as supplementary movies. The sets of figures [Figure 4, Figure 5] and [Figure 6, Figure 7] describe the conformations of the couples DA – β-TM (Figure 3) when the sliding speed is the lowest and the highest at this abscissa, respectively. In these figures, A and B refer to the calculation of the conformation of the couples DA – β-TM, assuming that the spatial frequencies of the β-TMs and DAs are either constant (in absence of JPI wave trains), or depend on the propagation of a JPI wave train, respectively. In C a DA grasps a β-TM only if these two partners are exactly facing, and the result is the same as that shown in B; this induces however, the formation of larger clusters of "inactive" activated DAs along the ODPs; in C, stand-by DAs were masked (Figure 3).

Figure 4 A[1], Figure 5 A[2], Figure 6 A[3], and Figure 7 A[4] show that in absence of variation of

[1] Movie S-2-A.
[2] Movie G-2-A.

the spatial frequencies of the two facing verniers, the couples are synchronized along very long segments, no matter of the ranks of the ODPs around the axonemal cylinder.

Figure 4 B[5], Figure 5 B[6], Figure 6 B[7], and Figure 7 B[8] show that JPI wave trains induce the formation of heterogeneous short clusters of synchronized DAs along the ODPs included in (or close to) the neutral surface (#3-4 and #8-9). In (or close to) the bending plane (*i.e.* ODP #1-2, #5-6 and #9-1), the couples are synchronized along longer clusters.

Addition of a stringent condition according to which the DAs have to be perpendicular to the ODPs when they grasp their facing partners (Figure 4 C[9], Figure 5C[10], Figure 6 C[11] and Figure 7 C[12]) does not change this result.

Along the 1 μm long segment located at the abscissa #2, the numbers of cycles achieved by the dynein arms (Figure 3) during a complete beating (under "B" conditions in the definition of Figure 1) equal: [1→2]: 259; [2→3]: 722; [2→3]: 951; [3→4]: 718; [5→6]: 1; [6→7]: 579; [7→8]: 882; [8→9]: 827; [9→1]: 514; the numbers in square brackets are the ranks of the two outer doublets included in a given pair. This shows that the largest numbers of cycles achieved by the DAs are those relative to the ODP located along the neutral surface; the lowest numbers are those of DAs located along the ODPs included in the bending plane (Cibert, 2002).

It is difficult to assign a length to the clusters constituted by the DAs along a given ODP during a complete beating cycle, because of the cyclical variations of the sliding speed and the consequences of these variations on the JPI wave trains. However, counting the DAs included into the clusters of different lengths along the 9 ODPs at a given abscissa, it is easy to calculate their cumulative occurrences during a complete beating cycle to estimate their obvious lengths.

When a cluster must include 2 DAs at least, the cumulative occurrences of the clusters of different lengths are presented in Figure 8. Because of the time resolution we have chosen (*i.e.* the time interval between two following images in the series that equals 1/8,000 s) and because no refractory period was defined in the cycle of the DAs, the numbers of isolated DAs are not taken into consideration in the calculation; these numbers decrease the total number of dynein arms possibly included into the clusters; then, the cumulative occurrence does not tend to 1 along the more active ODPs, excepted at the level of the P0 point (the 5th abscissa) where the sliding activity is the lowest. Thus, taking into consideration the cluster size for which the local maximum of DAs are recruited, Figure 8 shows that the lowest the activity of the ODP, the largest the maximum cluster length.

Even if the organization of the dynein arms is evidently not comparable to that of cilia, even if the molecular scaffolding that constitutes a dynein arm is evidently different in essence than the architecture of a cilium, it is amazing to observe that along a given ODP, the movements of the dynein arms included into successive clusters look like those of cilia along a given row. Is this comparison reasonable?

---

[3] Movie S-2-A.
[4] Movie G-2-A.
[5] Movie S-2-B.
[6] Movie G-2-B.
[7] Movie S-2-B.
[8] Movie G-2-B.
[9] Movie S-2-C.
[10] Movie G-2-C.
[11] Movie S-2-C.
[12] Movie G-2-C.

Cilia beat according to a metachronal coordination, a process that could be defined as: "the situation where *[cilia]* beat with a constant phase difference between adjacent rows in such way that tips form a moving pattern" (Gueron and Levit-Gurevich, 1998; Gueron and Levit-Gurevich, 1999), a mechanism that apparently involves the hydrodynamic coupling between the cilia. The apparent coordination of the dynein arms, that depends on the phase difference between the arms included in the cluster (Figure 5, Figure $7^{2,4,6,8,10,12}$) is due to the local probability of formation of the active couples DA – β-TM, which depends locally on the propagation of the JPI wave trains, which is not metachronal. In the case of cilia, metachronal coordination is energetically advantageous (Gueron and Levit-Gurevich, 1998; Gueron and Levit-Gurevich, 1999), and it could be interesting to interpret the apparent "metachronism" of the DAs within the clusters in the same terms, because the exact mechanism according to which the conformational changes are converted into mechanical energy and the yield of this intra-molecular process remains unknown, even if the forces produced by the DAs can be measured (Gennerich et al., 2007).

From a geometrical point of view, the apparent phase coherence of the dynein arms that allows us to define the clusters along a given ODP depends on the duration of the walking cycle, and on the local propagation of the JPI wave train that defines the probability of interaction between the two facing partners. The propagation of the clusters along ODP obeys evidently the two same basic events. On the other hand, from a physical point of view, the shift of phase exhibited by the dynein arms along a given cluster could be interpreted as the signature of the propagation of a dispersive wave, governed by a nonlinear dispersion relation, initiated locally by the JPI. The dispersion relation for such a wave is the relationship between the frequency, its wavelength and the length of the clusters, because it describes the balance between the neighbor interactions of DAs, and the dispersion tendencies of the ODP structure. A linear dispersion relation would suppress clusters stability and their equilibrium length, even if the geometry of the axoneme favors the formation of traveling localized clusters through JPI trains, also will favor the clusters to have the same phase difference between all the dynein arms (would be all in phase) and this was not observed, excepted along the ODPs whose sliding is always slow (*e.g.* the 5-6 pair, or at the level of the P0 point), or slows down because of the reversion of the sliding polarity. This has two obvious consequences.

First, the energy efficiency of the axoneme is obtained for a certain range of the length of the clusters and the capabilities of their included dynein arms to convert their conformational changes into force. It results that for any specific mechanical or hydrodynamic resistance the axoneme tunes to a certain optimal length and speed of the clusters displacement along the ODP such that the flow of energy is maximized. That is, the cluster velocity has its maximal possible value for a given geometry. Thus, the energy efficiency varies through a sort of (nonlinear) correlation between the arms included in a cluster and their activity, obtained by a lock-in of the energy flow inside each moving cluster. In this way the energy balance is fulfilled through the correlation between the external resistance, the length of the clusters (responsible for the consumed energy, and the potential energy of the dynein arms), and their velocity (responsible to the conversion of the conformational change — potential energy — into forces). These correlations remain to be studied.

Second, the JPI wave trains (that depend on the spatial frequencies of the two facing verniers and their sliding), the periodic distributions of the clusters along the ODPs, and the velocities of displacements of the clusters along the ODPs establish a 3 dimensional relation between space, time and frequency, governing thus he information that must propagate along and around the axonemal cylinder (Cibert, 2003).

Since observed clustering is mainly correlated to the local activity of the axoneme and the location of the ODP around the axonemal cylinder, it is not an intrinsic property of the dynein arms that would define *de facto* the number of arms that must form the clusters; it is an adaptative property of the couples DA – β-TMs, which looks like "local" cooperativity.

This raises four questions about the exact function of the ODPs around the axonemal cylinder. Do ODPs work only as springs? Is that the reason for which the 5-6 pair is apparently linked in a stable manner (Lindemann and Kanous, 1997)? Are the ODPs located only on both sides of the neutral surface (the most active one) the effective engines responsible for the bending of the axoneme? Are the physical properties of the outer doublets (and their adjustments) involved in the regulation of the activity of the dynein arms they carry (Cibert, C. submitted)?

The 3D bending of a cilium was modeled assuming that the dynein arms produce a force in a *given* direction only (Sugino and Naitoh, 1982). These authors have demonstrated that, under this condition, dynein arms form long active segments along the nine ODPs, and that these segments, along which the spatial frequencies of the DAs and β-TMs are constant, propagate clockwise and tipward along the axoneme. In the present study, the dynein arms are assumed to be able to tilt on both sides with respect to the baseward or tipward shear of the outer doublet pairs. Consequently, the clusters of active couples DA – β-TMs propagate along the ODPs with respect to the shear. These movements are not linked to the JPI wave trains that describe solely the spatial coincidence of each of the elements of the two facing verniers without any condition associated to their effective interaction.

The effects of the forces produced by the active couples upon the shape of the wave train that propagates along the axoneme are not taken into consideration here, because it has been postulated that the planar geometry of the flagellum integrates *on its own* the resultant of all the moments involved in the generation of this wave train. There is a corollary to this assumption. If the forces produced by the dynein arms would be used to create the same wave series, then their movements, and consequently the clusters they would form would be the same as those we have calculated. It is not trivial however to model an obvious relation between the longitudinal distributions of the active couples DA – β-TMs and the forces they are able to produce during the axonemal movement. This distribution can be either uniform (Camalet et al., 1999) or not (Sugino and Naitoh, 1982), considering two pioneer publications only. The longitudinal distributions of the active groups proposed by Sugino and Naitoh are compatible with the model presented here when the spatial frequencies of the two facing verniers are constant (panels A).

The corollary of the existence of long active segments propagating along, and around the axoneme, is the existence of inactive long segments, whose movements complement exactly those of the active ones. Thus, according to the assumptions proposed by Sugino and Naitoh, the distribution of the forces produced by the active couples DA – β-TMs appears to be very heterogeneous along, and around, the axoneme. In the present study, the mixing of short active and inactive segments could be correlated to a more homogeneous distribution of the forces produced by the active couples DA – β-TMs within the axoneme.

This comparison raises a question about the function of the nexin links, and of the radial spokes involved in the sliding-towards-bending conversion (Lindemann, 1994a; Lindemann, 1994b) because they make the axonemal scaffold to be partially cohesive (Gibbons, 1981). In effect, within long segments where the dynein arms are in stand-by conformation, the nexin links and the radial spokes become the only elements that insure the local cylindrical cohesion of the axoneme. If the links are not strong enough to insure this cohesion

function against some significant intensity of transverse-forces (Lindemann, 1994b), transient disruption of the axoneme may occur (Brokaw, 1997) and modify the local profile of the sliding-towards-bending conversion. Such a process could explain the observed variable shape of the wave train (Brokaw, 1965), because the distribution of the active dynein arms along and around the axoneme is one of the elements that define the shape of the wave train that propagates along the axoneme. Consequently, the wave trains depend on the swimming medium, the radial spokes, the nexin links, the outer doublets, and on the central pair, whose passive and active roles are necessarily linked.

In this context, Cibert, C., Toscano, J., Pensée, V. and Bonnet, G. have submitted a paper, whose topic is the calculation of the axonemal conformation when the organelle is submitted to internal constraints due to the activity of the dynein arms, the nexin links the radial spokes and the outer doublets, using finite elements approach. As expected, bending of the axoneme occurs *via* the creation of longitudinal and transversal tensions that modify the spatial distribution of the outer doublet within the axonemal cylinder itself. This is in agreement with the basic elements in the model proposed by Lindemann (Lindemann, 1994a; Lindemann, 1994b), even if the internal movements of the axoneme are opposite to those described by Lindemann (at least along the proximal segment of the axoneme).

The results described here do not deny at all the role of a molecular dialog of allosteric nature that must/could exist between the molecular complexes of the axoneme (Cibert, 2003). For example, in Chlamydomonas, it was demonstrated that the series of Outer Dynein Arms along a given doublet interact because of the fitment of their sub-units. Two different models, where the AAA systems (Roberts et al., 2009) play different functions, were proposed (Ishikawa et al., 2007). Using the same biological model, it was shown that AAA rings constitute the Inner Dynein Arms as well as the Outer Dynein Arms. It was confirmed that Inner Dynein Arms interact with the Outer Dynein Arms and the radial spokes, directly or via the Dynein Regulatory Complex (Bui et al., 2008).

This study complements the previous paper in which the JPI wave trains were described qualitatively (Cibert, 2008) and also reinforces the regulative function of sliding and curvature on their own regulation (Cibert, 2008; Lindemann and Lesich, 2010; Lindemann, 2004).

ACKNOWLEDGEMENTS

We thank Antonia Kropfinger and the referees who improved greatly the manuscript.

BIBLIOGRAPHY

Brokaw, C., 1996. Microtubule sliding, bend formation, and bend propagation parameters of *Ciona* sperm flagella altered by viscous load. Cell Motil. Cystoskel 33, 6-21.

Brokaw, C., 1997. Transient disruption of axonemal structure an microtubule sliding during bend propagation by Ciona sperm flagella. Cell Motil. Cytoskel. 37, 346-62.

Brokaw, C.J., 1965. Non-sinusoidal bending waves of sperm flagella. J Exp Biol 43, 155-69.

Brokaw, C.J., 1975. Effects of viscosity and ATP concentration on the movement of reactivated sea-urchin sperm flagella. J Exp Biol 62, 701-19.

Brokaw, C.J., 1993. Microtubule sliding in reduced-amplitude bending waves of Ciona sperm flagella: resolution of metachronous and synchronous sliding components of stable bending waves. Cell Motil Cytoskeleton 26, 144-62.

Bui, K.H., Sakakibara, H., Movassagh, T., Oiwa, K., and Ishikawa, T., 2008. Molecular architecture of inner dynein arms in situ in Chlamydomonas reinhardtii flagellum. J. Cell Biol. 183, 923-32.

Camalet, S., Jülicher, F., and Prost, J., 1999. Self-organized beating and swimming of internally driven filaments. Physical review letters 82, 1590-3.

Cibert, C., 2001. Elastic extension and jump of the flagellar nexin links: a theoretical mechanical cycle. Cell Motil. Cytoskel. 49, 161-75.

Cibert, C., 2002. Axonemal activity relative to the 2D/3D-waveform conversion of the flagellum. Cell Motility and the Cytoskeleton 51, 89-111.

Cibert, C., 2003. Entropy and information in flagellar axoneme cybernetics : a radial spokes integrative function. Cell motility and the Cytoskeleton 54, 296-316.

Cibert, C., 2008. Are the local adjustments of the relative spatial frequencies of the dynein arms and the tubulin monomers involved in the regulation of the "9+2" axoneme? Journal of Theoretical Biology 253, 74-89.

Dymek, E.E., and Smith, E., 2007. A conserved CaM- and radial spoke-associated complex mediates regulation of flagellar dynein activity. J. Cell Biol. 179, 515-26.

Fujime, S., Maruyama, M., and Fujime, S., 1972. Orientation distribution of globular protein molecules in a two-dimensional lattice: computer simulation. J. Theor. Biol. 36, 203-21.

Gennerich, A., Carter, A., Reck-Peterson, S., and Vale, R., 2007. Force-induced bidirectional stepping of cytoplasmic dynein. Cell 131, 952-65.

Gertsberg, I., Hellman, V., Fainshtein, M., Weil, S., Silberberg, S.D., Danilenko, M., and Priel, Z., 2004. Intracellular Ca2+ regulates the phosphorylation and the dephosphorylation of ciliary proteins via the NO pathway. J Gen Physiol 124, 527-40.

Gibbons, I., The molecular basis of flagellar motility in sea urchin spermatozoa, in: Inoué, S. and Stephens, R., Eds.), Molecular and cellular movement, Raven Press, New York 1975, pp. 207-32.

Gibbons, I.R., 1981. Cilia and flagella of eukaryotes. J. Cell Biol. 91, 1071-1245.

Goldstein, S., 1976. Form of developing bends in reactivated sperm flagella. J. Exp. Biol 64, 173-84.

Gray, J., 1955. The movement of sea-urchin spermatozoa. J. of Exptl. Biol. 32, 775-801.

Gray, J., 1958. The movement of spermatozoa of bull. J. Exp. Biol. 32.

Gray, J., and Hancock, G.J., 1955. The propulsion of sea-urchin spermatozoa. J. Exp. Biol. 32, 802-814.

Gueron, S., and Levit-Gurevich, K., 1998. Computation of the internal forces in cilia: application to ciliary motion, the effects of viscosity, and cilia interactions. Biophys J 74, 1658-76.

Gueron, S., and Levit-Gurevich, K., 1999. Energetic consideration of ciliary beating and

the advantage of metachronal coordination. Proc. Natl. Acad. Sci. USA 96, 12240-5.

Huang, B., Ramanis, Z., and Luck, D.J.L., 1982. Suppressor mutation in *Chlamydomonas* reveals a regulatory mechanism of flagellar function. Cell 28, 115-124.

Inaba, K., 2003. Molecular architecture of the sperm flagella: molecules for motility and signaling. Zoolog. Sci. 20, 1043-56.

Ishikawa, T., Sakakibara, H., and Oiwa, K., 2007. The architecture of outer dynein arms in situ. J. Mol. Biol. 368, 1249-58.

Li, C., Ru, C.Q., and Mioduchowski, A., 2006. Torsion of the central pair microtubules in eukaryotic flagella due to bending-driven lateral buckling. B.B.R.C. 351, 159-64.

Lindemann, C., 1994a. A "geometric clutch" hypothesis to explain oscillations of the axoneme of cilia and flagella. Journal of Theoretical Biology 168, 175-89.

Lindemann, C., and Kanous, K., 1997. A model for flagellar motility. Int. Review of Cytology 173, 1-72.

Lindemann, C., and Hunt, A., 2003. Does axonemal dynein push, pull or oscillate ? Cell Motility and the Cytoskeleton 56, 237-44.

Lindemann, C., and Lesich, K., 2010. Flagellar and ciliary beating: the proven and the possible. J. Cell Sci. 123, 519-28.

Lindemann, C.B., 1994b. A model of flagellar and ciliary functioning which uses the forces transverse to the axoneme as the regulator of dynein activation. Cell Mot. Cytoskel. 29, 141-54.

Lindemann, C.B., 2004. Testing the geometric clutch hypothesis. Biol Cell 96, 681-90.

Lindemann, C.B., 2007. The Geometric Clutch as a working hypothesis for future research on cilia and flagella. Ann N Y Acad Sci, 477-93.

Lindemann, C.B., and Mitchell, D.R., 2007. Evidence for axonemal distortion during the flagellar beat of Chlamydomonas. Cell Motil Cytoskeleton 64, 580-9.

Lorch, D.P., Lindemann, C., and Hunt, A., 2008. The motor activity of mammalian axonemal dynein studied in situ on doublet microtubules. Cell Motil Cytoskeleton 65, 487-94.

Mitchell, D., 2003a. Reconstruction of the projection periodicity and surface architecture of the flagellar central pair complex. Cell motility and the Cytoskeleton 55, 188-99.

Mitchell, D.R., 2003b. Orientation of the central pair complex during flagellar bend formation in Chlamydomonas. Cell Motil Cytoskeleton 56, 120-9.

Morita, M., Takemura, A., Nakajima, A., and Okuno, M., 2006. Microtubule sliding movement in tilapia sperm flagella axoneme is regulated by Ca(2+)/calmodulin-dependent protein phosphorylation. Cell Motil Cytoskeleton 63, 459-70.

Morita, Y., and Shingyoji, C., 2004. Effects of imposed bending on microtubule sliding in sperm flagella. Curr Biol 14, 2113-8.

Noguchi, M., Ogawa, T., and Taneyama, T., 2000. Control of ciliary orientation through cAMP-dependent phosphorylation of axonemal proteins in Paramecium caudatum. Cell Motility and the Cytoskeleton 45, 263-71.

Noguchi, M., Kitani, T., Ogawa, T., Inoue, H., and Kamachi, H., 2005. Augmented ciliary reorientation response and cAMP-dependent protein phosphorylation induced by glycerol in triton-extracted Paramecium. Zoolog Sci 22, 41-8.

Omoto, C., Palmer, J., and Moody, M., 1991. Cooperativity, in axonemal motion : analysis of a four-state, two-site kinetic model. Proc. Natl. Acad. Sci. USA 88, 5562-66.

Piperno, G., Mead, K., and Shestak, W., 1992. The Inner Dynein Arms I2 Interact with a "Dynein Regulatory Complex" in Chlamydomonas Flagella. J. Cell Biol. 118, 1455-63.

Roberts, A.J., Numata, N., Walker, M.L., Kato, Y.S., Malkova, B., Kon, T., Ohkura, R.,

Arisaka, F., Knight, P.J., Sutoh, K., and Burgess, S., 2009. AAA+ Ring and linker swing mechanism in the dynein motor. Cell 136, 395-6.

Rupp, G., and Porter, M., 2003. A subunit of the dynein regulatory complex in Chlamydomonas is a homologue of a growth arrest-specific gene product. J. Cell Biol. 162, 47-57.

Schoutens, J., 1994. Prediction of elastic properties of sperm flagella. Journal of theoretical biology 171, 163-77.

Smith, E., and Yang, P., 2004. The radial spokes and central apparatus : Mechano-chemical transducers that regulate flagellar motility. Cell Motil. Cytoskeleton 57, 8-17.

Spungin, B., Avolio, J., Arden, S., and Satir, P., 1987. Dynein arm attachment probed with a non-hydrolyzable ATP analog. Structural evidence for patterns of activity. J Mol Biol 197, 671-7.

Sugino, K., and Naitoh, Y., 1982. Simulated cross-bridge patterns corresponding to ciliary beating in Paramecium. Nature 295, 609-611.

Takano, Y., Yoshida, K., Kudo, S., Nishitoba, M., and Magariyama, Y., 2003. Analysis of small deformation of helical flagellum of swimming Vibrio alginolyticus : Bioengineering. JSME International Journal. Series C. 46, 1241-7.

Warner, F., Cross-bridge mechanism in ciliary motility: the sliding-bending conversion, in: Goldman, R., et al., Eds.), Cell Motility (Part C), Cold Spring Harbor Laboratory 1976, pp. 891-914.

Wilson, N.F., and Lefebvre, P.A., 2004. Regulation of flagellar assembly by glycogen synthase kinase 3 in Chlamydomonas reinhardtii. Eukaryot Cell 3, 1307-19.

Woolley, D., 2007. A novel motility pattern in quail spermatozoa with implications for the mechanism of flagellar beating. Biol Cell 99, 663-75.

Woolley, D.M., 1997. Studies on the eel sperm flagellum. I. The structure of the inner dynein arm complex. Journal of Cell Science 110, 85-94.

FIGURE CAPTIONS

Figure 1: **The modeled wave train**. **A** and **B** show 160 calculated flagellar traces where the difference between the phases of the periodic functions equal 0 and $\pi/2$, respectively; one trace in 10 is represented. **C**: The local extrema of the sum of the local shear along the 160 traces is clearly fish-shaped (Cibert, 2002). The five abscissas numbered 1, 2, 3, 4 and 5 are the sites where the conformations of the dynein arms were calculated; the abscissas defined as -1, -2, -3, +1, +2 and +3 refer to the abscissa #5 and were used to describe the relation between the local sliding speed and the local sum of the curvature through the fixed P0 point/segment. In **A**, **B** and **C** the ordinates are represented according to an arbitrary unit raging between -1 and +1.

Figure 2: **Scheme of the used cross-section of the axoneme**. The nine outer doublets were designed according to Schoutens (Schoutens, 1994) as proposed in our previous study (Cibert, 2008). Black arrows represent the DAs. The rank of each outer doublet is included within the tubule A. The bending plane includes the central apparatus of the axoneme and the center of inertia (Schoutens, 1994) of the first outer doublet. The green (positive) and the red (negative) values are the dilation and the compression of the spatial frequencies of the DAs and the β-TMs calculated in Cibert 2008, when the bending angle equals π along a 10 μm long segment. These values were calculated using the equation $s=\alpha*h$ (Warner, 1976), where s (Å) is the shear, α (rd) is the local curvature and h is the length (Å) of the projection in the bending plane of the distance that separates the axis of inertia of the outer doublet and either the end of the DA on one side or of the wall of the outer doublet on the other side; $h_{dynein} \in$ (89.10, 302.33, 397.75, 302.33, 79.46, 213.64, 373.39, 373.39, 207.46) and $h_{tubulin} \in$ (49.06, 167.49, 217.75, 163.30, 0.00, 114.99, 213.53, 192.18, 90.35); each value written in parentheses is associated to each of the outer doublets. This model could be used for any bending configuration changing the values of h_{dynein} and $h_{tubulin}$ as a function of the local change of the local orientation of the bending plane.

Figure 3: **Mechano-chemical cycle of the DAs with respect to the sliding amplitude of the ODPs**. The minus end of the ODP is oriented towards the left side of the scheme. The length of the DAs equals 180 Å; their interval ranges between 240 Å (outer DAs) to 320 Å (inner DAs) and change as a function of the curvature of the outer doublet. Under the conformation #1 activated but free DAs are able to grasp some β-TM along the facing vernier, as a function of their JPI; no refractory period was considered before the activated arm is able to grasp a facing partner. After the couple is formed, the tilt angle of the DA (the couple DA – β-TM) is calculated as a function of the amplitude of the local shear and of the maximal length of the walking distance. We postulate that, whatever the polarity of their movement (Lorch et al., 2008), the walking distances of the DAs have the same magnitude, and that the change of the sliding polarity does not induce the disruption of the link between the two partners. The horizontal curly brackets show five examples of clusters constituted by variable series of either unlinked dynein arms or active couples DA – β-TM of different lengths; because the formation of the active couples is time de-

pendent, the corresponding constituted clusters include arms whose tilt angles are different. Clusters of different lengths can form series along a given ODP.

Figure 4: **Series S-2-25**. Arbitrarily, S, 2 and 25 refer to the shear, the abscissa of the segment, and the rank of the image in the series, respectively. **A** refers to the standard calculation according to which efficient DA – β-TM couples were defined when the spatial frequencies of the two facing verniers are constant (in absence of compression/dilation equilibrium), no matter of the local curvature of the model. **B**, and **C** refer to the calculation of these couples accounting the incidence of the JPI wave train in the interaction between the two facing verniers. In **B**, the association between a DA and a facing β-TM is allowed when the relative locations of the two partner is calculated accounting a standard deviation that equals 27 Å. In **C**, the calculation assumes that the standard deviation is nil; in this case the stand-by DAs are not represented. The same conventions are used in Figure 5, Figure 6 and Figure 7. The rank #25 is that of the image where the sliding speed is the lowest in the series. The numbers located to the left and right sides of the images are the local sliding speed, the maximum walking distances of the DAs (during the forward (left) and the backward (right) phases of their mechano-chemical cycle), respectively. The sliding speed is positive or negative when the DAs are in the forward or the backward phase of their cycle, respectively. The series were calculated considering a 240 Å long interval between the DAs. No differences were observed when this interval was 320 Å long (not shown here). The trace of the axoneme is included on the left-hand side of the images; its proximal end is located at the top of the scheme. The segment of interest is represented on the trace by an open circle located as a function of its curvilinear abscissa.

Figure 5: **Series G-2-25**. Letter G refers to the groups of the DAs of similar conformations. When the conformation of the DA is almost vertical, the open circle is located on the horizontal blue line. The distance from any point to the blue line represents the tilt of the group. A DA not linked to a β-TM is not represented in this figure. Along a given cluster, the slope of the line shows that there is a phase difference between the cycles of the dynein arms depending on the different moments when the DA – β-TM couples are formed through the propagation of the JPI wave train.

Figure 6: **Series S-2-64**. The rank #64 corresponds to the highest sliding speed in the series (see Figure 4).

Figure 7: **Series G-2-64**. The rank #64 corresponds to the highest sliding speed in the series (see Figure 5).

Figure 8: **Cluster lengths**. Along each of the five 1 μm long segments of interest (Figure 1 C), for each ODP, and for the ensemble of 160 traces of the wave trains, the calculations are done as follows: if t is the rank of the trace, o is the rank of the outer doublet on which the DAs are permanently linked, and i is the number of active dynein arms involved in a cluster ($i \in [1, 44]$), the quantity $s_{i,t}$ for each of the ODP has the form:

$$s_{i,t} = \sum_{i,t} n_{i,t} x_{i,t} .$$

Then, we determine the maximum of the 9 sums obtained from the nine ODP

($\max_{i,o,t}$). The normalized occurrence of a class along a given outer doublet ($N_{i,o}$) equals:

$$N_{i,o} = 1 - \left(\frac{\max_{i,o,t} - n_{i,o} x_{i,o}}{\max_{i,o,t}} \right).$$

The cumulative occurrences of $N_{i,o}$ were calculated along each of the nine outer doublet and must range on the interval [0,1].

Figure 1

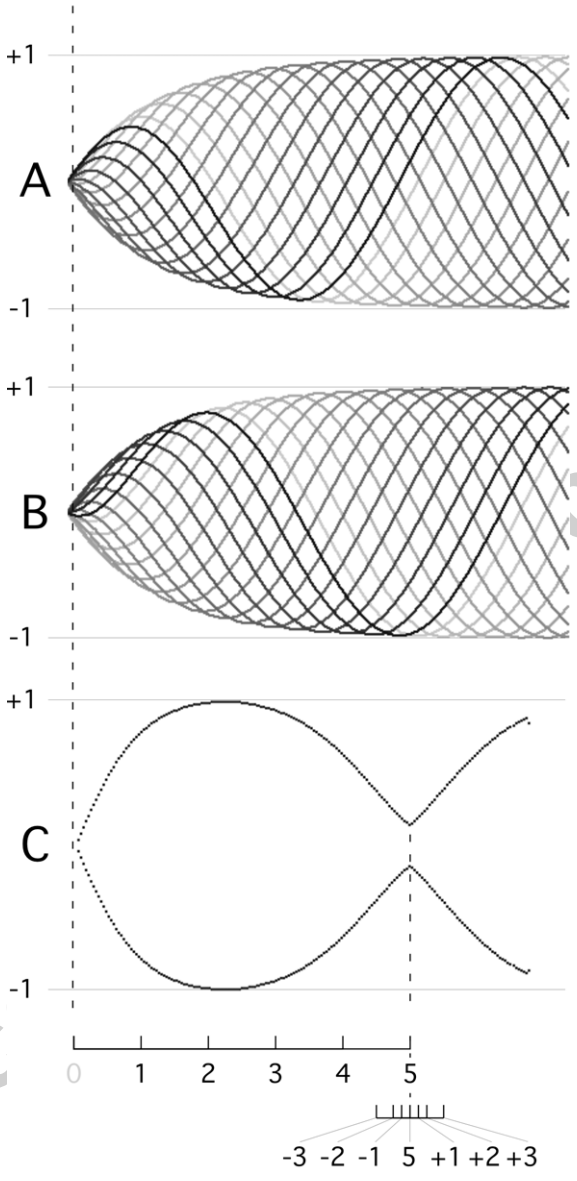

Figure 2

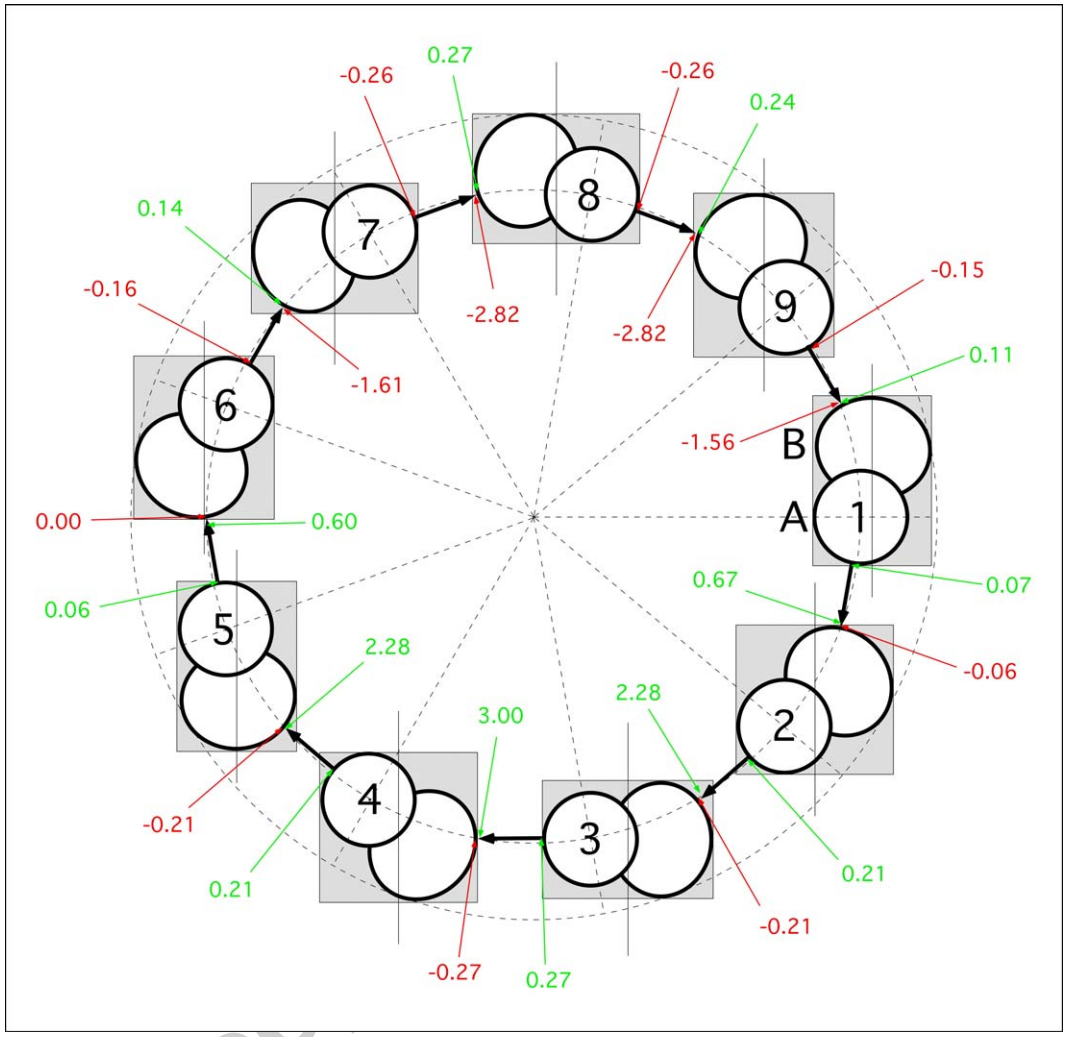

Figure 3

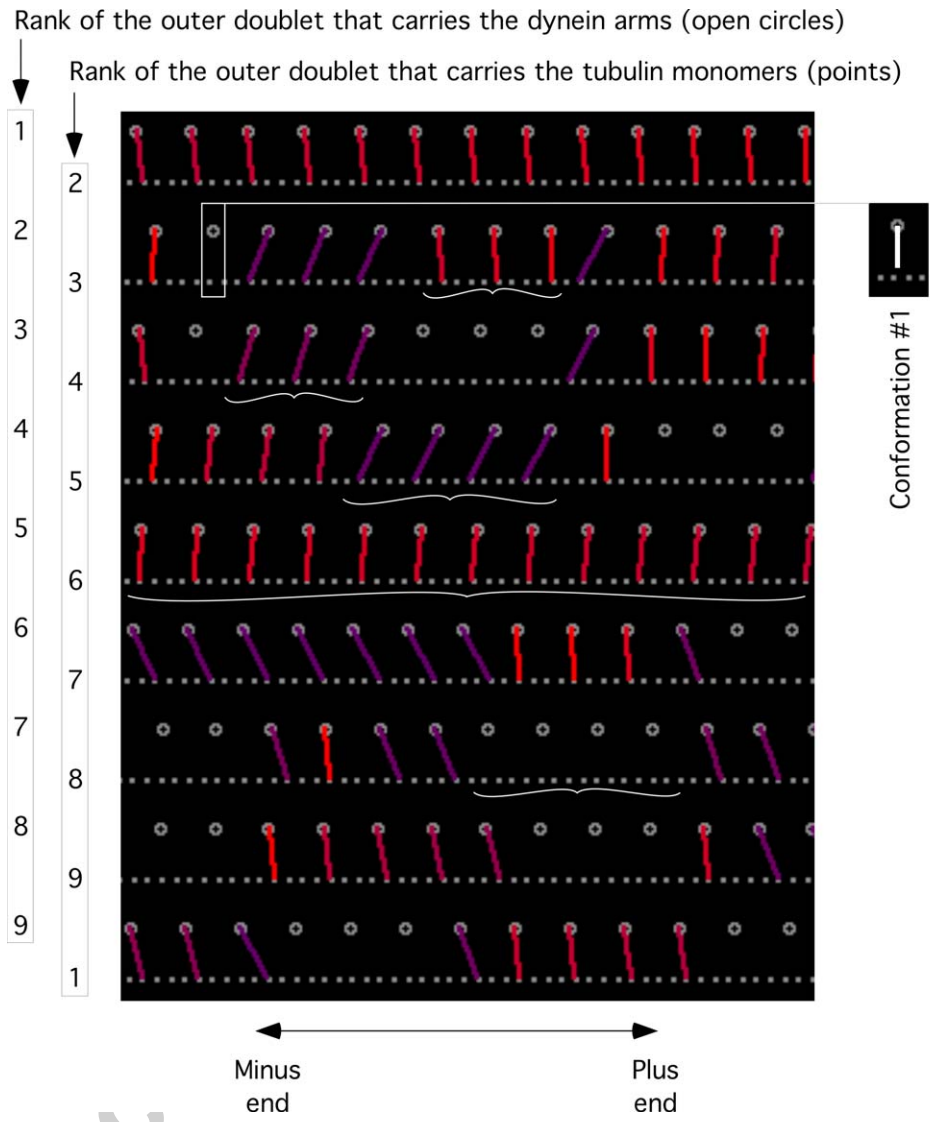

Figure 4

(S-2-25)

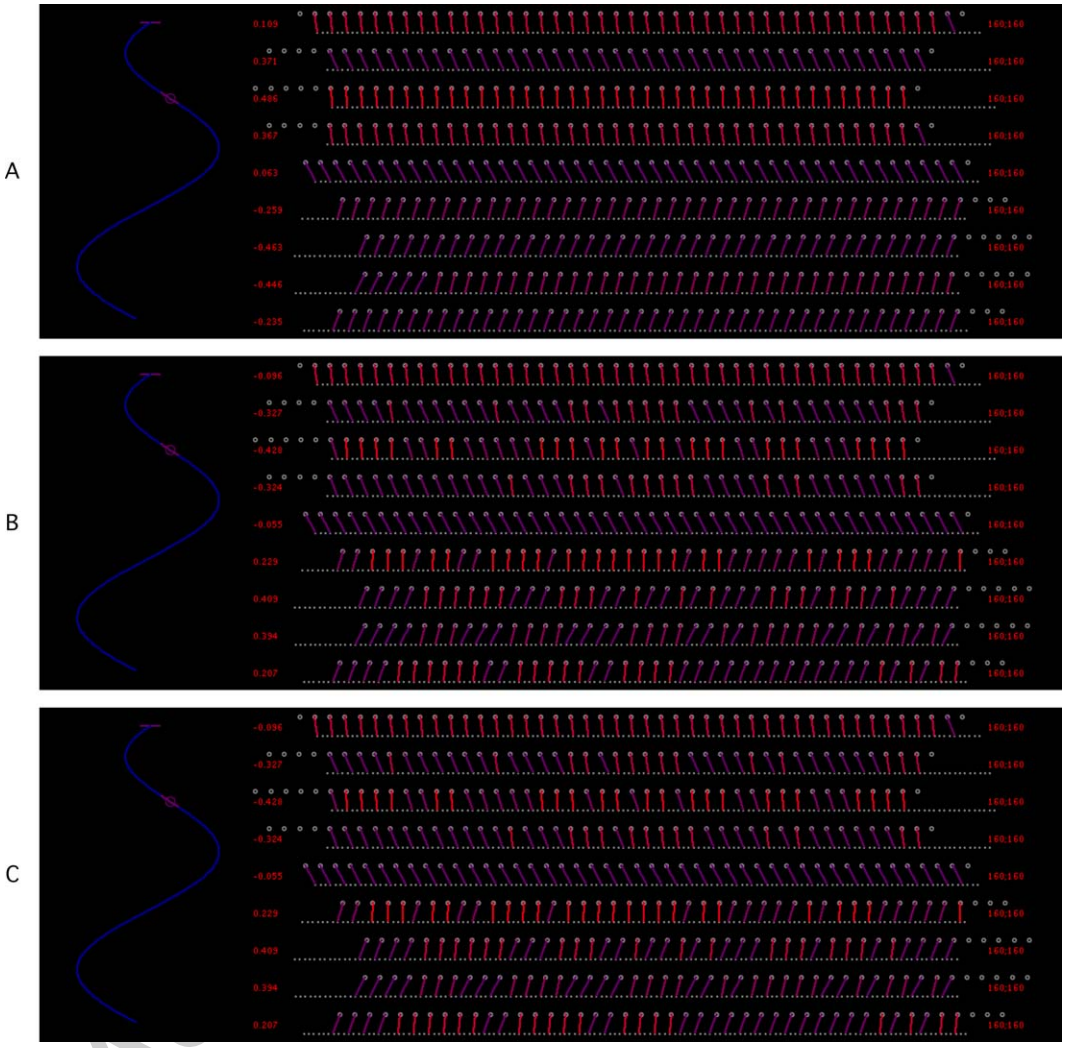

Figure 5

(G-2-25)

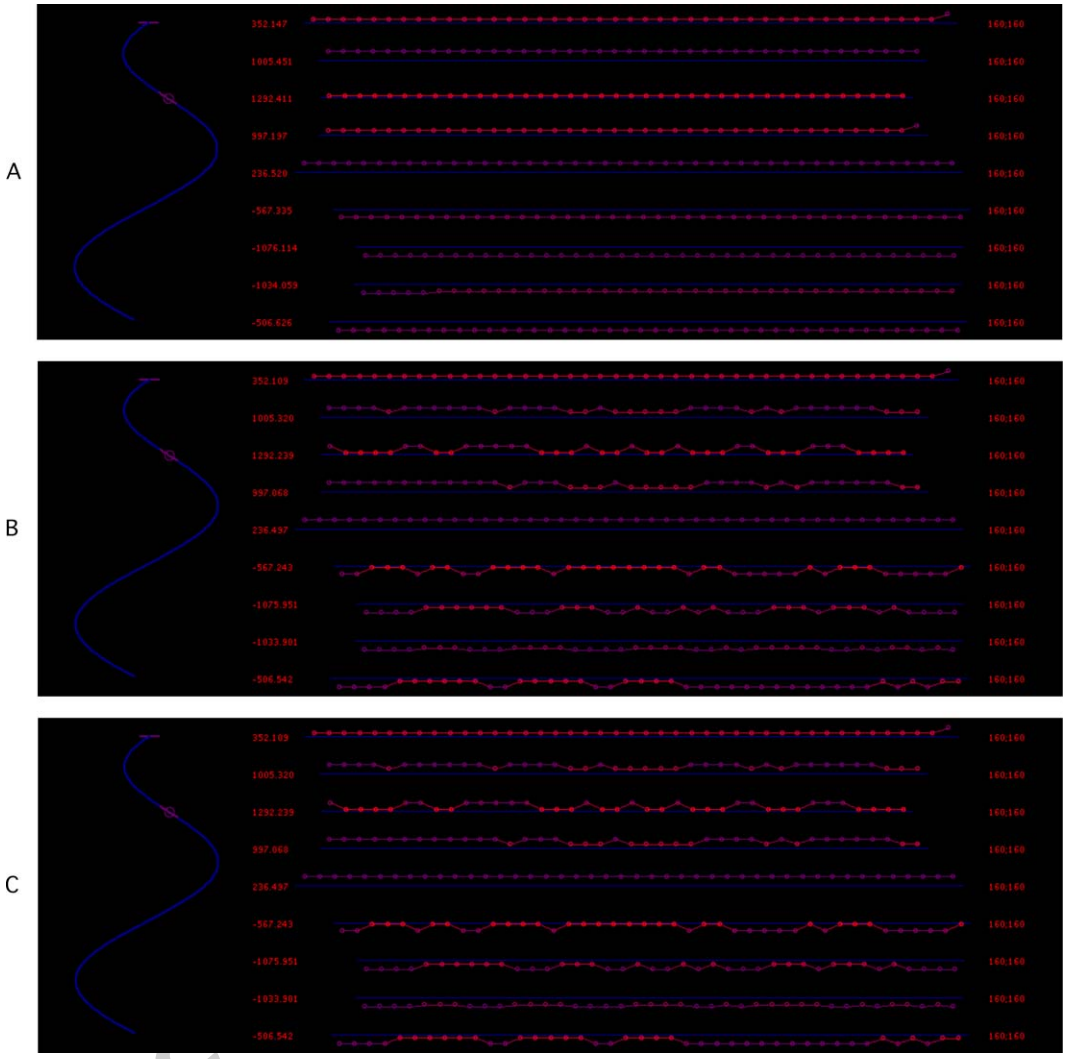

Figure 6

(S-2-64)

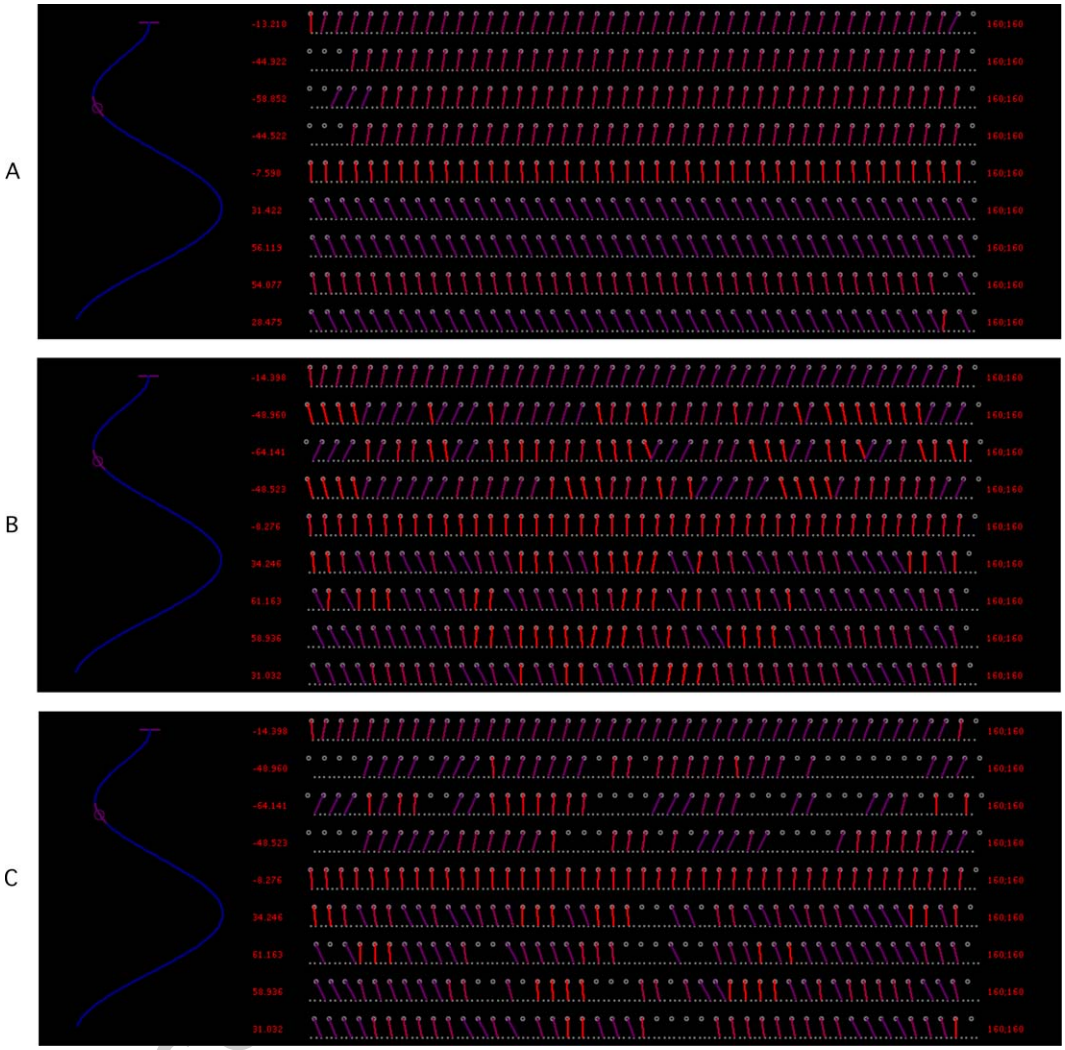

Figure 7

(G-2-64)

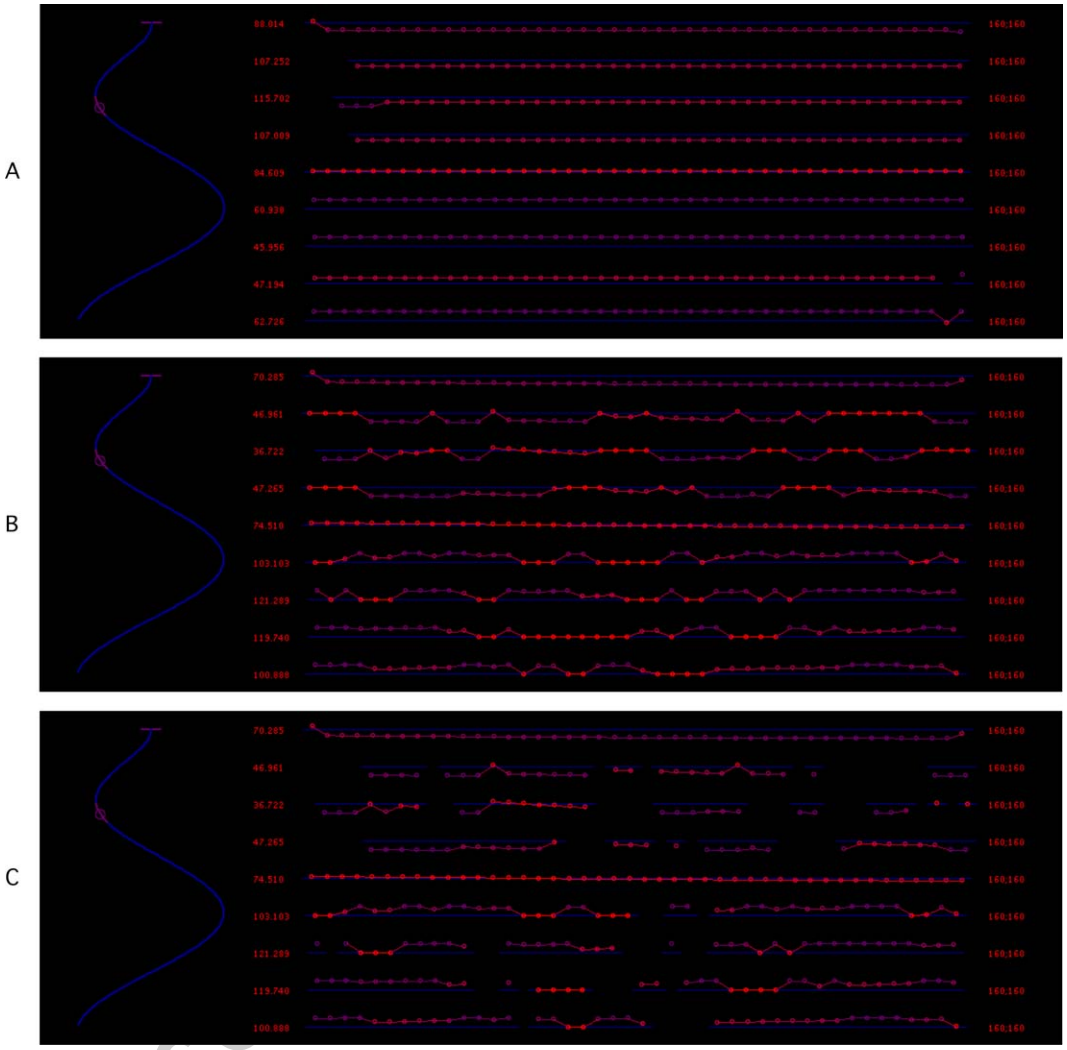

Figure 8